Published in:
Microscale Heat Transfer-Fundamentals and Applications,
S. Kakac, *et al.* (ed.), Kluwer
Academic Publishers (2005),
pp. 93-124.

MICROSCALE HEAT TRANSFER AT LOW TEMPERATURES*

RAY RADEBAUGH
Cryogenic Technologies Group
National Institute of Standards and Technology
Boulder, Colorado, USA

1. Introduction

This paper discusses the fundamentals and applications of heat transfer in small space and time domains at low temperatures. The modern trend toward miniaturization of devices requires a better understanding of heat transfer phenomena in small dimensions. In regenerative thermal systems, such as thermoacoustic, Stirling, and pulse tube refrigerators, miniaturization is often accompanied by increased operating frequencies. Thus, this paper also covers heat transfer in small time domains involved with possible frequencies up to several hundred hertz. Simple analytical techniques are discussed for the optimization of heat exchanger and regenerator geometry at all temperatures. The results show that the optimum hydraulic diameters can become much less than 100 μm at cryogenic temperatures, although slip flow is seldom a problem. The cooling of superconducting or other electronic devices in Micro-Electro-Mechanical Systems (MEMS) requires a better understanding of the heat transfer issues in very small sizes. Space applications also benefit from a reduction in the size of cryocoolers, which has brought about considerable interest in microscale heat exchangers. Some recent developments in miniature heat exchangers for Joule-Thomson and Brayton cycle cryocoolers are discussed. Both single-phase and two-phase heat transfer are covered in the paper, but the emphasis is on single-phase gas flow. Some discussion of fabrication techniques is also included.

Another application discussed here is the use of high frequency Stirling and pulse tube cryocoolers in smaller sizes and lower temperatures. This second area of microscale heat and mass transfer involves the short time scales experienced in high frequency oscillating thermodynamic systems. Models and empirical correlations for heat transfer and pressure drop obtained for steady-state flows in large systems need to be examined carefully in their use with very short time scales. Regenerative cryocoolers like the Stirling and pulse tube cryocoolers could be miniaturized much more than in current practice by utilizing high frequencies. However, the thermal penetration depths in both the gas and the regenerator matrix decrease with increasing frequency, which requires smaller hydraulic diameters for good heat transfer throughout the material in the short time available in a half cycle. These penetration depths in the helium working fluid become smaller at lower temperatures. This paper presents equations useful for the optimization of regenerator geometry that should be valid for temperatures down to about 50 K. The limitation on the maximum operating frequency and its effect on the miniaturization of regenerative cryocoolers is discussed.

2. Temperature, Heat Transfer, and Flow Regimes

Though most heat transfer phenomena to be discussed here apply to all temperatures, we focus mostly on applications dealing with the cryogenic temperature range. Cryogenic temperatures are defined loosely as those temperatures below about 120 K. However, in reaching these low temperatures part of the refrigeration cycle will be at room temperature, and in the heat exchanger the temperature will vary from room temperature to the low temperature. Thus, we need to consider heat transfer issues at temperatures that range from cryogenic up to room temperature for any cryogenic refrigeration process.

In this paper we consider two types of microscale heat transfer issues. The first issue pertains to size. Deviations from macroscale or continuum flow heat transfer behavior in gaseous flows will occur whenever the boundary layer begins to slip at the walls, thus the term slip flow is used to describe such flow. The Knudsen number *Kn*, which is the ratio of the molecular mean free path λ to the characteristic dimension of the channel, characterizes the type of flow. Continuum flow occurs when $Kn < 10^{-3}$. As *Kn* increases, the flow enters the slip flow regime ($10^{-3} < Kn < 10^{-1}$), transition flow regime ($10^{-1} < Kn < 10$), and eventually the free-molecular flow regime ($Kn > 10$) [1]. For nitrogen at atmospheric pressure and room temperature the mean free path is about 66 nm, and for helium it is about 194 nm. Thus, slip flow will begin to occur in nitrogen with channel diameters smaller than about 66 μm and in helium with diameters less than about 194 μm for room temperature and for atmospheric pressure. In some cases characteristic dimensions of flow channels in cryocoolers may be less than these critical values where slip begins to occur. However, for *Kn* less than 10^{-2} the effects on friction factors and Nusselt numbers are less than a few percent and can usually be ignored. In this paper we calculate values of Knudsen numbers that may occur in optimized heat exchangers for cryocoolers. Of particular interest is the case where these cryocoolers are scaled to miniature sizes. We generalize the definition of the microscale region to include all channel sizes with characteristic dimensions less than about 200 μm. Fabrication of such small channels often requires techniques different than those used in larger systems. Also two-phase flow often occurs in cryogenic refrigerators and bubble size then influences the design of flow channels.

The second microscale heat transfer issue considered in this paper deals with short time scales and their influence on the dimensions required for good heat transfer. Many cryocoolers use oscillating flows and pressures with frequencies as high as about 70 Hz. Heat flow at such high frequencies can penetrate a medium only short distances, known as the thermal penetration depth δ_t. Figure 1 shows how the temperature amplitude of a thermal wave decays as it travels within a medium. The distance at which the amplitude is 1/e of that at the surface is the thermal penetration depth, which is given by

$$\delta_t = \sqrt{(2k / \omega\rho c_p)}, \tag{1}$$

where *k* is the thermal conductivity, ω is the angular frequency, ρ is the density, c_p is the specific heat of the medium. In a similar manner the viscous penetration depth in a fluid is given by

$$\delta_\nu = \sqrt{(2\mu / \omega\rho)}, \tag{2}$$

where μ is the dynamic viscosity. These penetration depths indicate how far heat and momentum can diffuse perpendicular to the surface. Higher frequencies lead to smaller penetration depths. For good

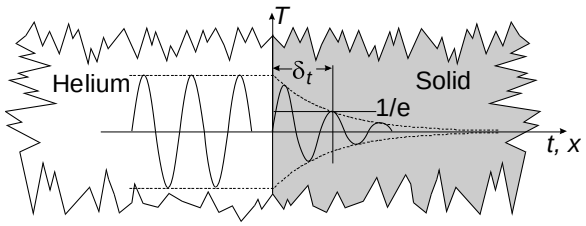

Figure 1. Schematic showing the decay of temperature amplitude inside a solid and the definition of thermal penetration depth.

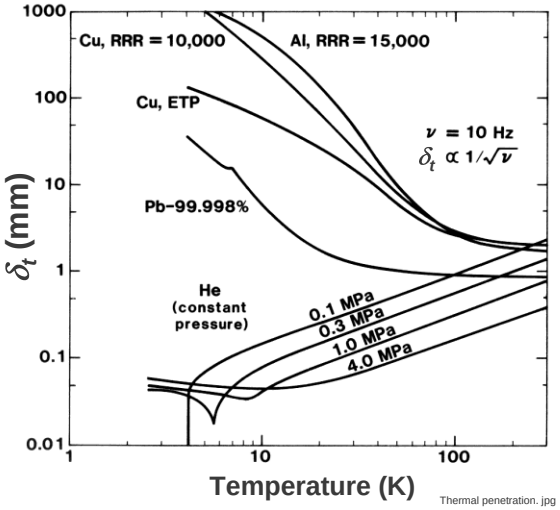

Figure 2. Thermal penetration depths at 10 Hz in helium and several pure metals.

heat transfer the lateral dimensions in the fluid or the solid must be much less than δ_t. In a fluid at distances much greater than δ_ν from a wall there is no viscous contact with the wall. Figure 2 shows the temperature dependence of the thermal penetration depth in helium and several pure metals for a frequency of 10 Hz. For pure metals oscillating heat flow can penetrate large distances because of their high thermal conductivity. However, for helium gas the thermal penetration depth is quite small, especially at low temperatures. Thus, hydraulic diameters in cryogenic heat exchangers for oscillating flow should be less than about 100 μm for frequencies greater than about 10 Hz.

An additional complication that occurs with oscillating flow is the existence of several regimes of laminar and turbulent flow that are functions of frequency as well as Reynolds number, as shown in Figure 3 for the case of smooth circular tubes [2]. These flow regimes are the subject of much research [3]. They are shown as a function of the peak Reynolds number $N_{r,\,peak}$ and the ratio of channel radius R to the viscous penetration depth δ_ν. This ratio is sometimes referred to as the dynamic Reynolds number and is similar to the Womersley number ($Wo = D/\sqrt{2}\delta_\nu$). In the weakly turbulent regime

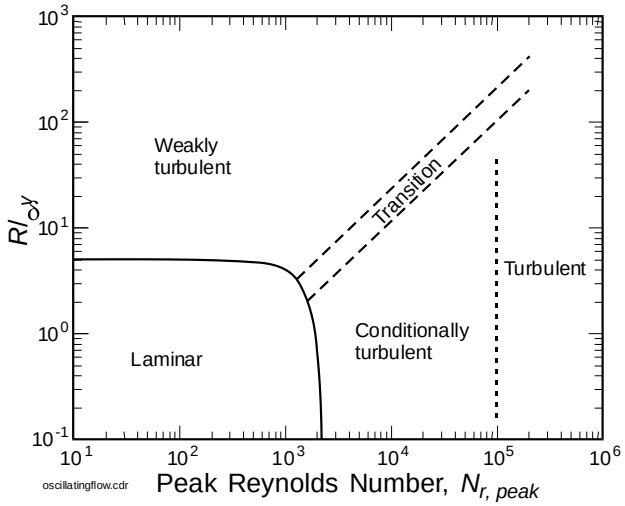

Figure 3. Regimes of oscillating flow in a smooth circular pipe as a function of peak Reynolds number and ratio of pipe radius R to viscous penetration depth δ_ν [2].

turbulence occurs only in the center of the channel and not at the boundary. In the conditionally turbulent region turbulence occurs at the peak velocity and changes back to laminar or weakly turbulent when the velocity crosses through zero.

3. Cryogenic Refrigeration Techniques

3.1 CONVENTIONAL REFRIGERATION

The refrigeration techniques required to reach cryogenic temperatures are different than those of conventional vapor-compression refrigeration, which is used for most cooling applications closer to ambient temperatures. Most domestic refrigerators and air conditioners use the vapor-compression cycle. Figure 4a shows a schematic of the vapor-compression cycle, and Figure 4b shows the path of the cycle in the temperature-entropy (*T*-*S*) diagram. In this cycle heat is absorbed at some low temperature during the boiling of the liquid at a pressure near 0.1 MPa (1 bar). Typically the temperatures may be about 250 K (-23 °C) for most domestic refrigerators. At this temperature oil can remain dissolved in the refrigerant and not freeze. The vapor being boiled off in the evaporator then passes to the oil-lubricated compressor where it is compressed to about 2.5 MPa (25 bar). As the compressed vapor travels through the condenser it cools to ambient temperature and condenses into the liquid phase. The oil used for lubrication of the compressor is soluble in the refrigerant and a small amount of oil then completes the entire refrigerant cycle dissolved in the refrigerant. The condensed liquid then passes to the expansion capillary where the pressure is reduced to about 0.1 MPa and the temperature drops from ambient to about 250 K during this isenthalpic process between c and d in Figure 4.

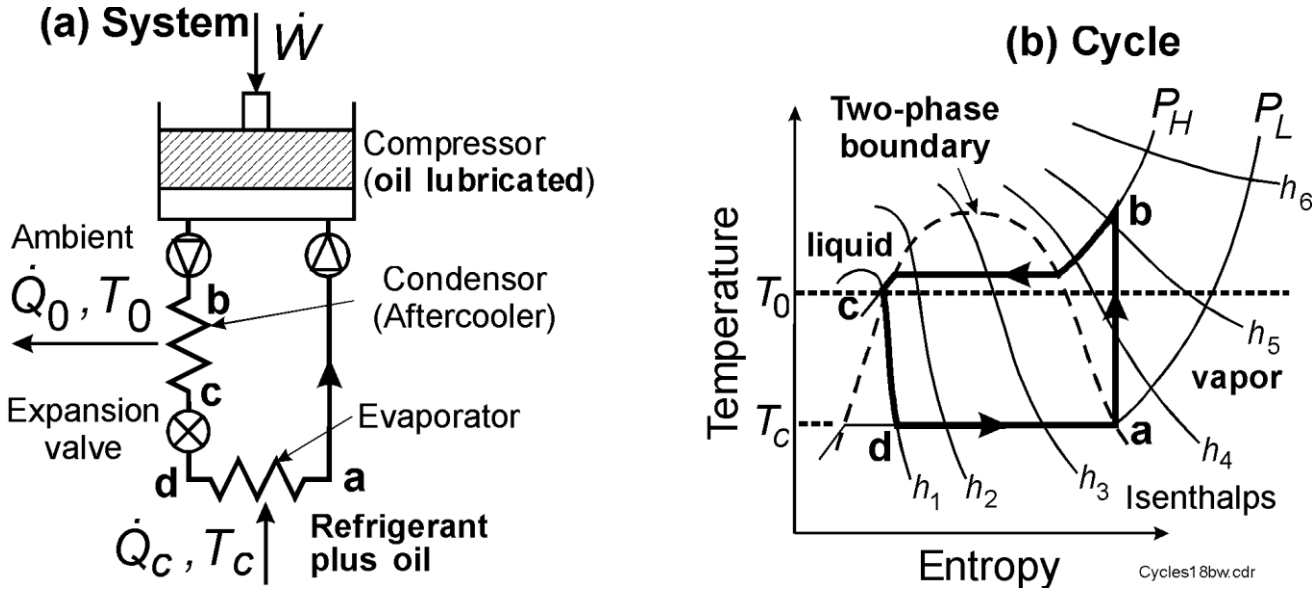

Figure 4. (a) Schematic of the vapor-compression cycle with an oil-lubricated compressor. (b) The vapor-compression cycle shown on a temperature entropy diagram operating between a low pressure P_L and a high pressure P_H and between a low temperature T_c and ambient temperature T_0.

3.2 RECUPERATIVE CYCLES

To achieve cryogenic temperatures, for example 80 K, the process shown in Figure 4 must be modified in two ways. First, the solubility of lubricating oil in the working fluid at such low temperatures is extremely small and any excess will freeze and cause plugging of the expansion channels. Thus, either the compressor must be oil free, which introduces reliability issues, or the system must have oil removable equipment utilizing complex processes (cost issues) to remove the oil before it reaches such low temperatures. Second, no fluid exists which can be expanded in an isenthalpic process (no expansion work) from room temperature to cryogenic temperatures. Even with a work-recovery process the initial pressure would need to be impractically high to achieve such low temperatures after expansion. Thus, it is necessary to precool the high-pressure gas in a heat exchanger prior to the expansion, as is shown schematically in the Joule-Thomson cryocooler in Figure 5a. The path followed on the *T*-S diagram is shown in Figure 5b. Because the heat transferred in the heat exchanger to provide sufficient precooling is much larger than the refrigeration power, the effectiveness of the heat exchanger must be very high, often higher than 95%. Small hydraulic diameters are needed in the heat exchanger to obtain such high effectiveness, especially for miniature cryocoolers. Hydraulic diameters of 50 to 100 μm may be required in some compact heat exchangers. When an expansion engine or turbine replaces the expansion orifice the cycle is called the Brayton cycle. Both it and the Joule-Thomson cryocooler are classified as recuperative types because of the use of recuperative heat exchangers throughout the cycle.

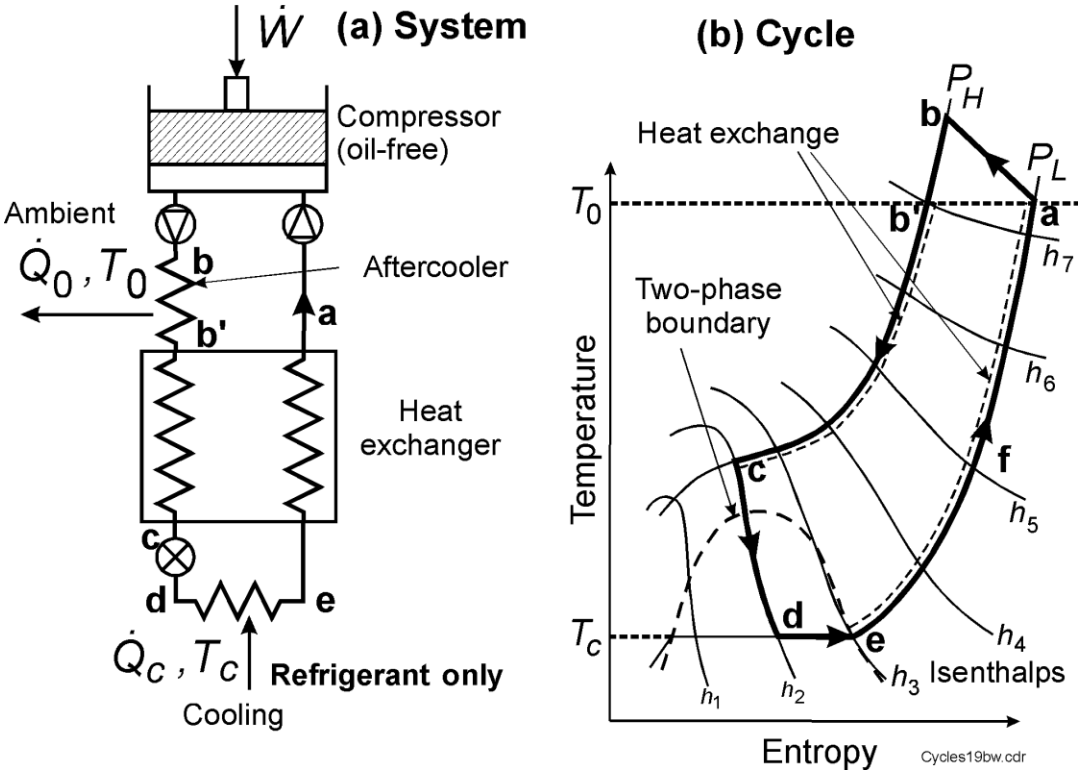

Figure 5. (a) Schematic of the Joule-Thomson cryocooler showing the use of an oil-free compressor and a high-effectiveness heat exchanger. (b) The Joule-Thomson cycle shown on a temperature-entropy diagram. Dashed lines indicate the heat exchange process in the heat exchanger.

3.3 REGENERATIVE CYCLES

In the past 20 years or so cryogenic temperatures are more commonly achieved by the use of regenerative cryocoolers. These cryocoolers, shown as schematics in Figure 6, operate with oscillating pressure and flow. They have at least one regenerative heat exchanger, or regenerator, where the hot and cold streams flow in the same channel, but at different times. Heat is stored for a half cycle in the heat capacity of the matrix. The Stirling cryocoolers and some pulse tube cryocoolers typically operate at about 20 to 70 Hz frequency and have no valves in the compressor. The Gifford-McMahon (GM) cryocoolers and some pulse tube cryocoolers operate at about 1 to 2 Hz frequency. The lack of valves in the higher frequency Stirling crycoolers and some pulse tube cryocoolers give them higher efficiencies than those of the valved systems. Thus, there is much emphasis on these higher frequency systems, particularly for space and miniature applications. For a constant power the size of the system decreases as the frequency increases. However, there are heat transfer problems at the higher frequencies that will be discussed here. More complete descriptions of the various cryocooler cycles are given by Radebaugh [4, 5].

4. Applications of Cryocoolers

We present here a few examples of cryocooler applications to show where microscale heat transfer issues at low temperatures may be of some concern. The overall size of the cryocooler usually has little bearing on whether microscale heat transfer issues are involved. It is the hydraulic diameter that is important in determining microscale effects. Small hydraulic diameters are required for very effective heat exchangers, particularly for those used in high frequency regenerative cryocoolers. For

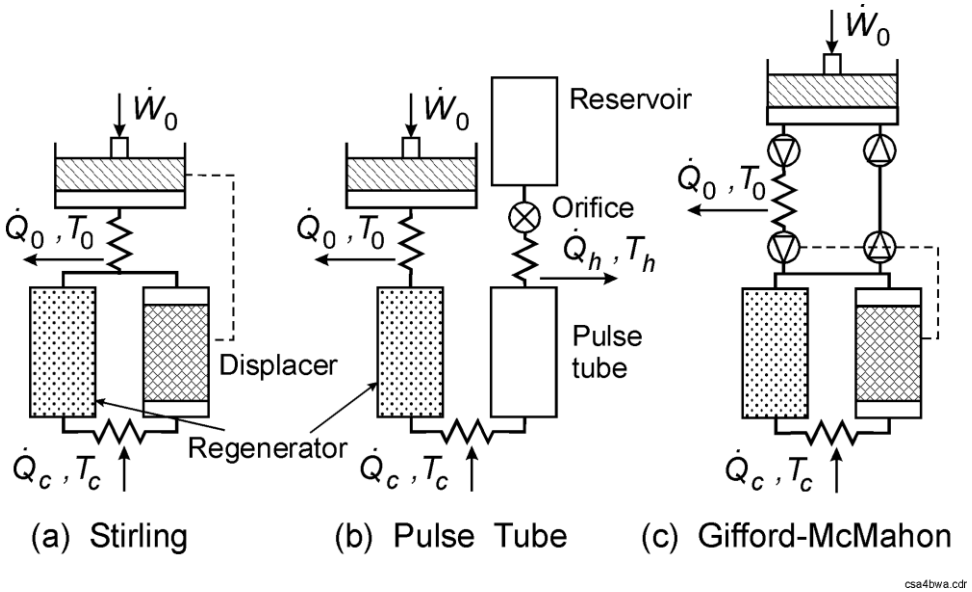

Figure 6. Schematics of the three common regenerative cryocoolers. The Stirling cryocooler (a) uses a valveless compressor or pressure oscillator and has a moving displacer operating synchronously with the piston. The pulse tube cryocooler (b) has no displacer in the cold head. The Gifford-McMahon cryocooler (c) uses a valved compressor with oil lubrication and oil removal equipment.

recuperative heat exchangers high effectiveness can still be achieved with large hydraulic diameters, but the overall size of the heat exchanger becomes large. Thus, we concentrate on applications with more compact cryocoolers. The cooling of infrared sensors to about 80 K for high-resolution night vision, primarily for the military has been one of the largest applications of cryocoolers. Figure 7 shows the cold heat exchanger and expansion orifice of a small Joule-Thomson cryocooler used to rapidly cool (few seconds) infrared sensors in the guidance system of missiles. Miniature finned tubing is used for the heat exchanger. Because there are no moving parts at the cold end of the Joule-Thomson cryocooler it can be scaled down to very small sizes. There is growing interest in developing such a cooler using MEMS technology for a cooler on a chip that might provide a few milliwatts of cooling at 80 to 100 K. We shall examine the optimization of the heat exchanger geometry for this application in the next section.

The infrared sensors on tanks, helicopters, airplanes, etc. are usually cooled to 80 K with miniature Stirling cryocoolers operating at about 50 to 60 Hz frequency. Over 140,000 such coolers have been made to date for this application [4]. Hydraulic diameters of about 50 to 60 μm are generally used in the packed-screen regenerators to obtain high effectiveness. The same hydraulic diameter and length would be used in much larger Stirling or pulse tube cryocoolers to obtain the same regenerator effectiveness. Only the cross-sectional area of the regenerator should be scaled with the refrigeration power. The smallest commercial Stirling cryocooler is shown in Figure 8. It is used primarily for commercial applications of infrared sensor cooling to 80 K, such as for process monitoring. Only 3 W of input power are required for this cooler to produce 0.15 W of cooling at 80 K. Somewhat larger Stirling cryocoolers (6 W at 77 K), shown in Figure 9, provide cooling for high-temperature superconducting microwave filters used in some cellular phone base stations for enhanced sensitivity. Over 3000 base stations now use superconducting filters (~1% of the total).

Figure 10 shows a miniature pulse tube cooler developed for cooling infrared sensors or high-T_c superconducting electronics in space applications. It provides about 0.5 W of cooling at 80 K. With this particular cooler the regenerator and the pulse tube are inline. The cold surface is in the middle between these two components. In addition to military applications the cooled infrared sensors in space are being used for studies of atmospheric phenomena, such as the ozone hole, green-house effect, and long-range weather forecasting. To gain greater sensitivity to long-wavelength infrared radiation

Figure 7. Joule-Thomson micro cryocooler. Courtesy APD Cryogenics.

Figure 8. Stirling micro cryocooler that provides 0.15 W of cooling at 80 K with 3 W of input power. Courtesy Inframetrics/FLIR Systems.

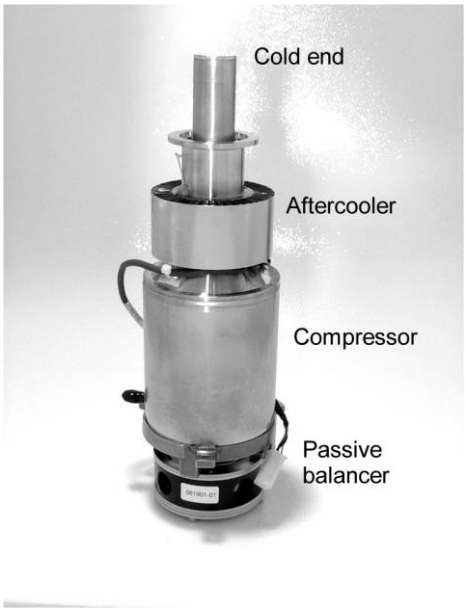

Figure 9. Stirling cryocooler used for cooling high-Tc superconducting microwave filters to 77 K in mobile phone base stations. Courtesy STI.

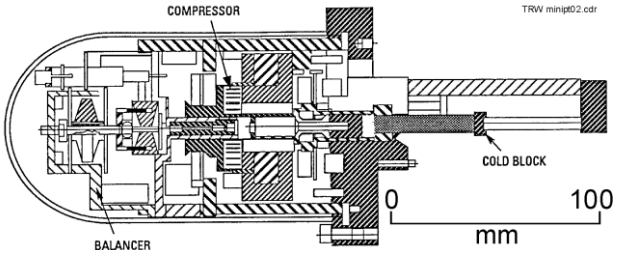

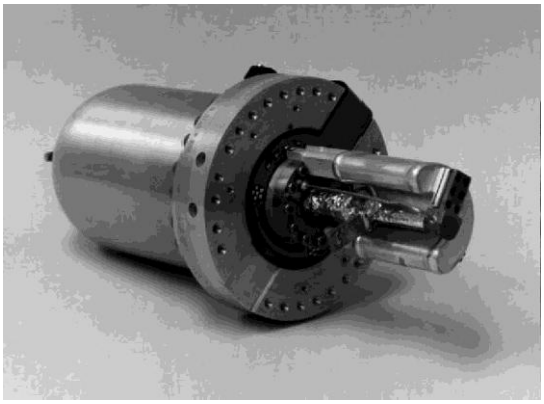

Figure 10. Mini pulse tube cryocooler used for cooling infrared sensors or superconducting devices in space. Courtesy TRW/NGST.

for astronomy missions space agencies are now pushing for cryocoolers to reach temperatures of 10 K or lower. To maintain liquid hydrogen fuel in space for long-range exploration missions there is now a growing need for efficient and compact 20 K cryocoolers. The pulse tube cryocooler is being considered for these new applications, but there is a need to better understand the heat transfer problems in regenerators at these low temperatures and at high frequencies. Frequencies of at least 20 Hz are required to keep the compressor small. As shown in Figure 2 the thermal penetration depth for this frequency in helium at a pressure of about 2 MPa and temperatures of 20 K and below is about 50 μm. The hydraulic diameter within the regenerator should then be significantly less than that value for good heat transfer. Such small hydraulic diameters are challenging to achieve in practice, particularly with parallel plates or tubes. With packed spheres the resulting void volume (38%) is higher than optimum for these low temperatures, and there is difficulty in containing such small spheres under oscillating flow conditions.

5. Optimization of Heat Exchanger Geometry

Our objective in optimizing the heat exchanger geometry is minimizing the volume of the heat exchanger. That objective is particularly important for the development of micro cryocoolers. The heat exchanger is usually the largest component of the Joule-Thomson cryocooler, except for the compressor. Of interest here is the value of the Knudsen number in optimized micro cryocoolers. In the optimization procedure we choose to fix the fractional losses associated with imperfect heat transfer, pressure drop, and axial heat conduction. These losses are normalized by the gross refrigeration power $\dot{Q}_r$ of the cryocooler. The pressure drop in a flow channel of cross-sectional area A_g, length L, and hydraulic diameter D_h is given by

$$\Delta P = \frac{2 f_r (\dot{m} / A_g)^2 L}{\rho D_h}, \tag{3}$$

where f_r is the Fanning friction factor, $\dot{m}$ is the mass flow rate in the flow channel, and ρ is the density of the gas. The density should be evaluated at the average temperature. We can relate the friction factor to the Stanton number N_{St}, a dimensionless heat transfer number, by the Reynolds analogy

$$\alpha = \frac{N_{St} N_{Pr}^{2/3}}{f_r}, \tag{4}$$

where N_{Pr} is the Prandlt number and α is a dimensionless number that is a function of the geometry. Figure 11 shows how α varies with the Reynolds number for various geometries. The behavior of the Stanton number and the friction factor discussed here are based on experiments with macrosystems in continuum flow [6]. We note that α is a rather weak function of the Reynolds number, which makes the optimization procedure being described here very simple and powerful. Radebaugh and Louie [7] describe details of this procedure for regenerators. Both f_r and N_{St} are strong functions of Reynolds number but the ratio is only a weak function. The Stanton number is defined as

$$N_{St} = \frac{h}{(\dot{m} / A_g) c_p}, \tag{5}$$

where h is the heat transfer coefficient and c_p is the specific heat of the gas at constant pressure. We can proceed with the optimization by taking α to be a specific number independent of the Reynolds

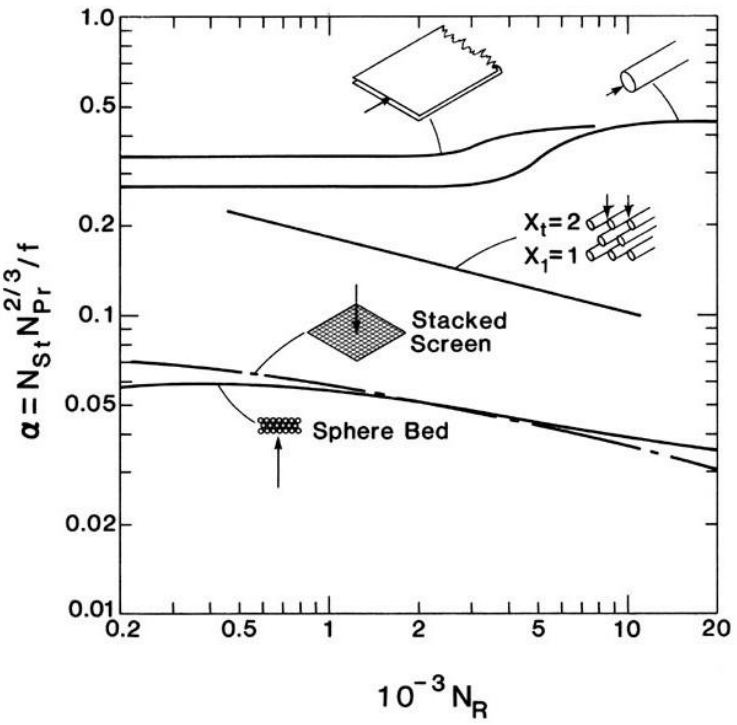

Figure 11. Reynolds analogy for several geometries as a function of the Reynolds number [6].

number, which is not known at this point in the optimization.

By substituting equation (4) into equation (3) we can express the pressure drop in terms of the heat transfer parameter N_{St} as

$$\Delta P = \frac{2 N_{St} N_{Pr}^{2/3} (\dot{m} / A_g)^2 L}{\alpha \rho D_h}. \tag{6}$$

The number of heat transfer units N_{tu} on any given side of the heat exchanger is

$$N_{tu} = \frac{hA}{\dot{m} c_p}, \tag{7}$$

where A is the surface area for heat transfer on one side of the heat exchanger. The surface area A is related to the hydraulic diameter through the definition of hydraulic diameter by

$$D_h \equiv 4 L A_g / A. \tag{8}$$

By combining equations (5), (7), and (8) we have

$$N_{tu} = 4 N_{St} L / D_h. \tag{9}$$

By using equation (9) to find N_{St} and substituting it into equation (6) the pressure drop becomes

$$\Delta P = \frac{N_{tu} N_{Pr}^{2/3} (\dot{m} / A_g)^2}{2 \alpha \rho}. \tag{10}$$

5.1 GAS CROSS-SECTIONAL AREA

After rearranging equation (10) the specific cross-sectional area is then given by

$$\frac{A_g}{\dot{m}} = \left[\frac{N_{tu} N_{Pr}^{2/3}}{2 \alpha \rho \Delta P} \right]^{1/2}. \tag{11}$$

The problem with equation (11) is that we do not know *a priori* a reasonable design value for N_{tu} on each side of the heat exchanger. A more fundamental design parameter would be the heat loss associated with the imperfect heat exchanger compared with the gross refrigeration power. The heat exchanger ineffectiveness (1 - ε), where ε is the effectiveness, is defined by

$$1 - \varepsilon = \frac{\dot{Q}_{hx}}{\dot{m} (h_h - h_c)_{\min}}, \tag{12}$$

where $\dot{Q}_{hx}$ is the heat flow or loss to the cold end due to imperfect heat transfer in the heat exchanger, h_h is the specific enthalpy of the gas at the hot end, and h_c is the specific enthalpy of the gas at the cold end. The subscript min refers to the stream (high or low pressure) with the minimum difference in specific enthalpy between the hot and cold ends. Figure 12 shows the specific enthalpy curves for

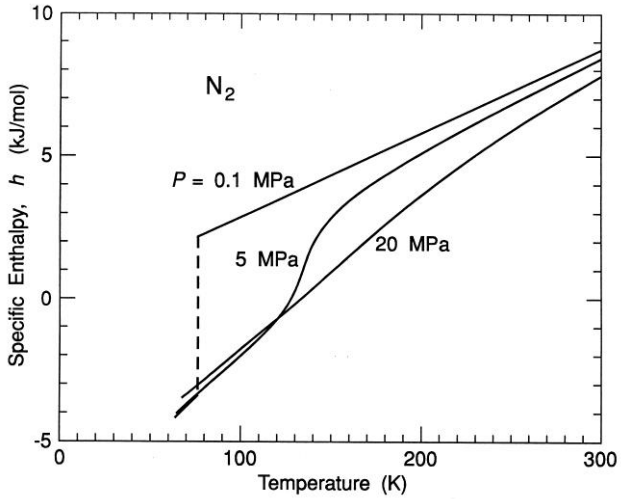

Figure 12. Specific enthalpy of nitrogen for different pressures.

nitrogen for two different pressures. As shown by these curves the minimum enthalpy difference occurs in the low-pressure stream. The gross refrigeration power provided by the Joule-Thomson cryocooler is given by

$$\dot{Q}_r = \dot{m}\Delta h_{\min}, \tag{13}$$

where $\Delta h_{\min}$ is the minimum difference in specific enthalpy between the high and low pressure. As shown in Figure 12 this minimum for nitrogen occurs at the warm end of the heat exchanger. The specific heat exchanger loss and the specific refrigeration power can be defined as

$$q_{hx} = \dot{Q}_{hx} / \dot{m} \qquad\qquad q_r = \dot{Q}_r / \dot{m} = \Delta h_{\min}. \tag{14}$$

We can combine equations (12) and (13) to obtain

$$1 - \varepsilon = (\dot{Q}_{hx} / \dot{Q}_r) q_r^*, \tag{15}$$

where q_r^* is the ratio of the refrigeration power to the heat flow in the heat exchanger, or relative refrigeration power, as given by

$$q_r^* = \frac{q_r}{(h_h - h_c)_{\min}}. \tag{16}$$

We note from equation (15) that q_r^* is the maximum allowed value of 1 - ε, that is $(\dot{Q}_{hx} / \dot{Q}_r)$ must be less than 1 to allow for any net refrigeration. If $q_r^* < 1$, a heat exchanger is required to yield any net refrigeration power. That condition usually is a distinguishing feature of cryocoolers compared with vapor-compression refrigerators.

The ineffectiveness of a heat exchanger and the associated heat flow to the cold end as given by equation (12) are normally associated with the complete heat exchanger. The number of heat transfer units for the complete heat exchanger is given by

$$\frac{1}{N_{tu0}} = \frac{1}{N_{tu1}} + \frac{1}{N_{tu2}}, \tag{17}$$

where N_{tu1} and N_{tu2} are the number of heat transfer units on each side of the heat exchanger. Published curves [6] and tables give the ineffectiveness (1 - ε) as a function of N_{tu0}. For $N_{tu0} > 10$ (a necessity for nearly all cryocooler heat exchangers) the heat exchanger ineffectiveness, is approximated very well by

$$1-\varepsilon = B/N_{tu0}, \tag{18}$$

where the constant B is given by $B = 1$ whenever the specific heats in both streams are equal. If they are not equal, equation (18) can still be used by making $B < 1$, but in that case B becomes somewhat a function of N_{tu0} [7]. For B independent of N_{tu0} or a weak function of it, we can expand equation (18) according to equation (17) into

$$1-\varepsilon = \frac{B}{N_{tu1}} + \frac{B}{N_{tu2}} = (1-\varepsilon)_1 + (1-\varepsilon)_2, \tag{19}$$

where each side has its own ineffectiveness and associated heat flow $\dot{Q}_{hx}$ according to equation (15).

By using equation (15) to represent each side of the heat exchanger equation (19) allows us to express N_{tu} for each side of the heat exchanger as

$$N_{tu} = \frac{B}{(\dot{Q}_{hx}/\dot{Q}_r)q_r^*}, \tag{20}$$

where $(\dot{Q}_{hx}/\dot{Q}_r)$ now is the relative heat flow from each side of the heat exchanger. We substitute this expression for N_{tu} into equation (11) to obtain the specific gas cross-sectional area for one side as

$$\frac{A_g}{\dot{m}} = \left[\frac{BN_{Pr}^{2/3}}{2\alpha\rho q_r^* \Delta P(\dot{Q}_{hx}/\dot{Q}_r)}\right]^{1/2}. \tag{21}$$

Equation (21) gives the specific area in terms of the relative heat loss, which is a better design parameter than the number of heat transfer units used in equation (11). However, for highly unbalanced heat capacity flows the actual overall heat loss will deviate from the sum of the individual losses used in these calculations. The more accurate heat loss for the complete heat exchanger is given by equation (15) when the overall ineffectiveness is found from the N_{tu0} evaluated from the individual N_{tu} by equation (17). In this expression the density ρ is a strong function of temperature.

For an ideal gas we use the relation

$$\rho = P/RT, \tag{22}$$

where R is the gas constant per unit mass and T is the absolute temperature. For an ideal gas, equation (21) can then be written as

$$\frac{A_g}{\dot{m}} = \left[\frac{BRTN_{Pr}^{2/3}}{2\alpha P_0^2 q_r^* (\Delta P/P_0)(\dot{Q}_{hx}/\dot{Q}_r)}\right]^{1/2}, \tag{23}$$

where P_0 is the average pressure within the flow channel being optimized. The temperature should be taken as the average between the hot and cold ends of the heat exchanger. Equation (23) can be converted to a molar flow basis by replacing R with MR_0, where M is the gas molecular weight and R_0 is the universal gas constant 8.314 J/(mol·K).

In order to obtain any finite refrigeration power each of the loss terms ($\Delta P/P_0$) and ($\dot{Q}_{hx}/\dot{Q}_r$) should be sufficiently small. Heat flow to the cold end by axial conduction $\dot{Q}_{cond}$ is the remaining loss that must be considered in the optimization of the heat exchanger geometry. We will use that later in the calculation of the optimum length. The pressure drop causes a loss in the refrigeration power that can be denoted as $\dot{Q}_{\Delta P}$. In order to have a finite net refrigeration power the losses must satisfy the condition

$$(\dot{Q}_{\Delta P}/\dot{Q}_r)_1 + (\dot{Q}_{hx}/\dot{Q}_r)_1 + (\dot{Q}_{cond}/\dot{Q}_r)_1 + (\dot{Q}_{\Delta P}/\dot{Q}_r)_2 + (\dot{Q}_{hx}/\dot{Q}_r)_2 + (\dot{Q}_{cond}/\dot{Q}_r)_2 < 1, \qquad (24)$$

where the subscripts 1 and 2 refer to the two sides of the heat exchanger. Typically the losses on each side must be less than about 0.5. The relationship between ($\Delta P/P_0$) and ($\dot{Q}_{\Delta P}/\dot{Q}_r$) depends on the refrigeration cycle and the operating conditions. For the Joule-Thomson cycle the ratio of the two terms is given by

$$\frac{(\dot{Q}_{\Delta P}/\dot{Q}_r)}{(\Delta P/P_0)} = \frac{P_0}{\Delta h_{\min}}\left(\frac{\partial h}{\partial P}\right)_T, \qquad (25)$$

where the partial derivative should be evaluated at the same temperature as $\Delta h_{\min}$. The ratio in equation (25) may vary from about 0.6 to 1.2 on the high pressure side of most Joule-Thomson systems. However, the low pressure side may be much more complicated. In most cases the ratio in equation (25) for the low pressure side may only be 0.3 or smaller. For pure gases the specific heats of the two streams are not equal and $\Delta h_{\min}$ occurs at the high temperature end. Thus, expanding the gas at the cold end only to the pressure where the enthalpy change is the same as $\Delta h_{\min}$ and allowing for a pressure drop through the low pressure side of the heat exchanger forces the enthalpy change in both sides of the heat exchanger to be equal. In that case there is no loss of refrigeration power, but with the balanced heat exchanger the value of *B* will be 1 rather than some lower value.

For a practical cooler the sum of the normalized loss terms in equation (24) should usually be less than about 0.6, which can be satisfied with each individual loss being about 0.1. In that case an approximate upper limit for the product $(\Delta P/P_0)(\dot{Q}_{hx}/\dot{Q}_r)$ in equation (23) is about 0.01 for the high pressure stream. An important aspect of equation (23) to note is that the right hand side is independent of the flow rate or size of the refrigerator. Thus, equation (23) shows that the proper scaling relationship for the gas cross-sectional area A_g is for it to be proportional to the flow rate, which is also proportional to the refrigeration power.

5.2 HEAT EXCHANGER LENGTH

Equation (23) shows that the volume of the heat exchanger could be made as small as desired by making the length small. However, in that case the conduction loss $\dot{Q}_{cond}$ becomes large. The conduction loss on each side of the heat exchanger is given by

$$\dot{Q}_{cond} = (A_s/L)\int_{T_c}^{T_h} k\,dT, \qquad (26)$$

where A_s is the cross-sectional area of the solid structure of the flow channel. We shall ignore the thermal conduction through the gas. The term A_s is related to A_g through the porosity n_g by

$$n_g = \frac{A_g}{A_s + A_g}. \tag{27}$$

The heat exchanger length for a given conduction loss on each side is expressed as

$$L = \frac{(A_g / \dot{m})(1 - n_g)\int k dT}{n_g q_r (\dot{Q}_{cond} / \dot{Q}_r)}. \tag{28}$$

As to be expected, the length can be made small by decreasing the solid fraction ($1 - n_g$), but the strength of the material containing the gas imposes a limit to how high the porosity can be made. For a circular tube with internal pressure P the minimum solid fraction can be taken as

$$(1 - n_g) = 2P / \sigma, \tag{29}$$

where σ is the maximum allowable tensile stress in the tube wall.

5.3 HEAT EXCHANGER VOLUME

The gas volume in the heat exchanger is given by combining equation (28) with equation (21), or with equation (23) for an ideal gas. For the general case the gas volume becomes

$$\frac{V_g}{\dot{m}} = \frac{A_g L}{\dot{m}} = \frac{BN_{Pr}^{2/3}(1 - n_g)\int k dT}{2\alpha n_g q_r^* q_r \rho \Delta P (\dot{Q}_{hx} / \dot{Q}_r)(\dot{Q}_{cond} / \dot{Q}_r)}. \tag{30}$$

The volume per unit of gross refrigeration can be expressed as

$$\frac{V_g}{\dot{Q}_r} = \frac{BN_{Pr}^{2/3}(1 - n_g)\int k dT}{2\alpha n_g q_r^* q_r^2 \rho \Delta P (\dot{Q}_{hx} / \dot{Q}_r)(\dot{Q}_{cond} / \dot{Q}_r)}. \tag{31}$$

The total volume of the heat exchanger is given by dividing V_g by n_g. We note that in these last two equations that the volume of the heat exchanger is made small by maximizing α. Values of α for several different geometries are shown in Figure 11. As this figure shows parallel plates will produce the smallest gas volume, with parallel tubes giving slightly larger volumes. Because α is nearly independent of Reynolds number, the volume determined by this optimization procedure is also independent of the Reynolds number.

5.3 HYDRAULIC DIAMETER

We now derive the hydraulic diameter of the heat exchanger that must be used to achieve the area, length, and volume given above with the specified thermal loss in the heat exchanger. By multiplying equation (9) by $N_{Pr}^{2/3}$ we obtain

$$N_{St}N_{Pr}^{2/3} = \frac{N_{tu}N_{Pr}^{2/3}D_h}{4L}. \tag{32}$$

By using equation (4) we obtain

$$\alpha f_r = \frac{N_{tu}N_{Pr}^{2/3}D_h}{4L}. \tag{33}$$

The Reynolds number is given as

$$N_r = \frac{D_h}{\mu(A_g/\dot{m})}, \tag{34}$$

where μ is the viscosity. For every geometry of interest there is some function g where

$$f_r = g(N_r). \tag{35}$$

Combining equation (33) with equation (35) yields

$$\frac{N_{tu}N_{Pr}^{2/3}D_h}{\alpha 4L} = g(N_r). \tag{36}$$

Equation (36) is nonlinear and can be solved for D_h by trial and error in the most general form. However, for laminar flow it becomes linear and is easily solved. In laminar flow the function g becomes

$$g(N_r) = b/N_r, \tag{37}$$

where b is a constant that depends only on the geometry and is sometimes called the Poiseuille number. For long parallel plates b = 24, for long square tubes b = 14.25, for long circular tubes b = 16, and for long triangular tubes b = 13.33 [6]. These numbers correspond to the use of the Fanning friction factor. Equations (36) and (34) are solved in the laminar flow regime by

$$D_h = \left[\frac{4\alpha b\mu(A_g/\dot{m})L}{N_{tu}N_{Pr}^{2/3}}\right]^{1/2}. \tag{38}$$

Each term in equation (38) has been calculated previously. The solution to D_h then allows the Reynolds number to be calculated from equation (34). With this known value of the Reynolds number a new and more precise value of α could be determined from Figure 11 and the calculations repeated if more accuracy is desired. Because α is only a weak function of the Reynolds number the second calculation is seldom necessary. Equation (38) is expressed in terms of the original variables as

$$D_h = \left[\frac{2b\mu(1-n_g)\int k dT}{n_g\rho q_r \Delta P(\dot{Q}_{cond}/\dot{Q}_r)}\right]^{1/2}. \tag{39}$$

For the case where the density is given by an ideal gas equation of state equation (39) becomes

$$D_h = \left[\frac{2b\mu RT(1-n_g)\int k dT}{n_g P_0^2 q_r (\Delta P / P_0)(\dot{Q}_{cond} / \dot{Q}_r)} \right]^{1/2} . \quad (40)$$

It is interesting to note that D_h is independent of the thermal loss in the heat exchanger $\dot{Q}_{hx}$. It is also independent of the size of the heat exchanger. For a minimum volume the hydraulic diameter is independent of the flow rate, volume, or refrigeration power of the cryocooler. According to equation (21) only the cross-sectional area varies proportional to the flow rate. For some common geometries the relation between the hydraulic diameter, defined by equation (8), and the characteristic dimension is given by

Gap thickness $t_g = D_h / 2$ (41)

Tube diameter: $d = D_h$ (42)

Square channel side: $s = D_h$ (43)

Equilateral triangle side: $s = \sqrt{3} D_h$ (44)

Sphere diameter: $d = \frac{3D_h(1-n_g)}{2n_g}$ (packed spheres) (45)

Wire diameter: $d \approx D_h(1-n_g)/n_g$. (stacked screen) (46)

The practical porosity n_g of most packed spheres is about 0.38, and that of most commercial screen is about 0.65.

Equation (40) shows that the optimum hydraulic diameter decreases at lower temperatures. Thus, microscale effects may be more important in low temperature applications, such as in heat exchangers of cryocoolers. However, temperature has little effect on the relative importance of slip flow. The mean free path of gas molecules is given by

$$\lambda = 3.62 \frac{\mu}{P} \sqrt{\frac{T}{M}}, \quad (47)$$

where M is the molecular weight and the units are: λ (m), μ (Pa·s), P (Pa), T (K), and M (kg/mol). The Knudsen number $Kn = \lambda/D_h$ for an optimized flow channel in a heat exchanger will vary with temperature only through the temperature dependence of viscosity and the thermal conduction integral.

5.4 EXAMPLES

We now consider some examples to illustrate the geometries that minimize the volume of cryocooler recuperative heat exchangers. In all cases we use a conservative calculation with the constant $B = 1$. For case A we consider an ideal refrigeration cycle using helium gas with isothermal compression at 320 K and isothermal expansion at some low temperature T_c. The low pressure P_1 is 0.3 MPa and the high pressure P_2 is 0.6 MPa. We then optimize a heat exchanger operating between T_c and some high temperature T_h where $T_h = 4T_c$. We assume there is some other perfect heat exchanger

between T_h and the compressor at 320 K. The specific refrigeration power provided by the reversible isothermal expansion is given by

$$q_r = \dot{Q}_r / \dot{m} = RT_c \ln(P_2 / P_1) \tag{48}$$

For this case where $T_h = 4T_c$ the normalized specific refrigeration power q_r^* becomes (2/15)ln(P_2/P_1). For the pressure ratio of 2 considered here we have $q_r^* = 0.0924$. This value is rather high for such a low pressure ratio, but can only be achieved with reversible isothermal expansion. Such a process can only be approximated in practice and is particularly difficult to accomplish in miniature sizes. Values of the input parameters for all the examples are summarized in Table 1. For the examples used here we consider parallel plate geometry. For case A we assume both sides have a porosity of 0.5 initially. Figure 13 gives the specific cross-sectional areas calculated from equation (21) for the two gas streams as a function of the cold-end temperature. The dashed line is for the high-pressure stream when the length and width of that stream are made the same as that of the low-pressure stream. To force such dimensions the porosity on the high-pressure side was made 0.39 and the reduced heat exchanger loss was made 0.063. Figure 14 shows the temperature dependence of the heat exchanger lengths when both sides have a porosity of 0.5. Figure 15 shows the gap thickness for the two sides, including the case where the high-pressure side is forced to have the same length and width as the low-pressure side. The Knudsen number at the average temperature is shown in Figure 16. At the high temperature end of the heat exchanger the Knudsen number will be about $\sqrt{2}$ higher. This figure shows that at the warm end of heat exchangers at the lowest temperature slip flow may just begin to occur, but because *Kn* is less than 10^{-2} there is very little effect on the friction factor and the heat transfer coefficient. Figure 17 shows the width of the gap for the particular case where the mechanical input power is 1 W, which provides a flow rate of 2.17 mg/s. The figure also shows the temperature variation of the resulting gross refrigeration power. If the refrigeration power at 80 K were reduced by two orders of magnitude to about 2 mW, then the gap width is reduced to 30 μm, which is less than the gap thickness of about 50 μm on the low-pressure side. The optimization procedure described here then begins to become invalid for such small sizes.

A few other examples are examined here to illustrate the range of geometries that may exist in optimized heat exchangers for cryocoolers. These examples are for Joule-Thomson cryocoolers, which are easily miniaturized. Table 1 lists the operating conditions and important input parameters for all of

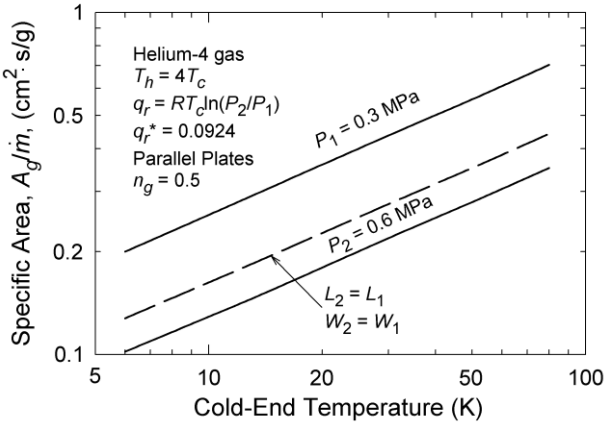

Figure 13. Gas cross-sectional area per unit mass flow rate as a function of cold-end temperature for case A.

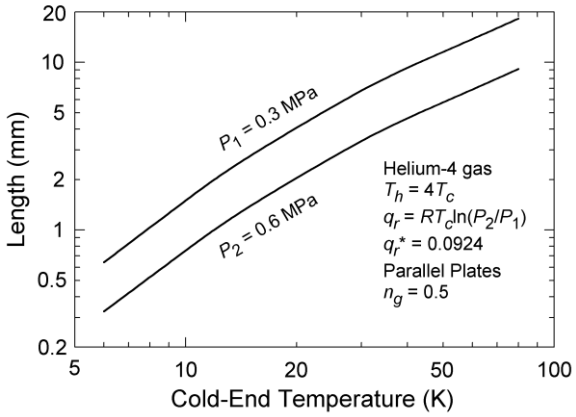

Figure 14. Calculated optimum length of heat exchanger of case A as a function of cold-end temperature.

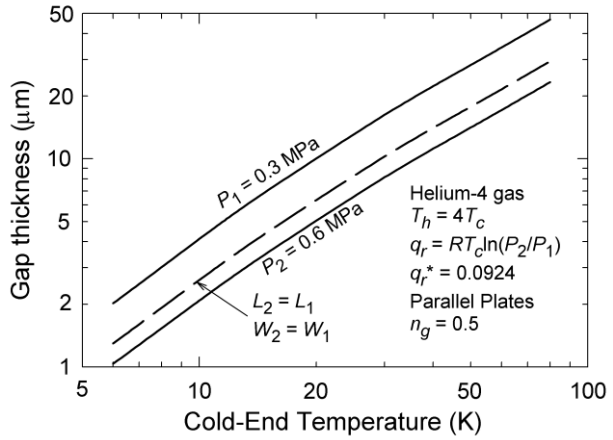

Figure 15. Optimum gap thickness between parallel plates for case A as a function of cold-end temperature.

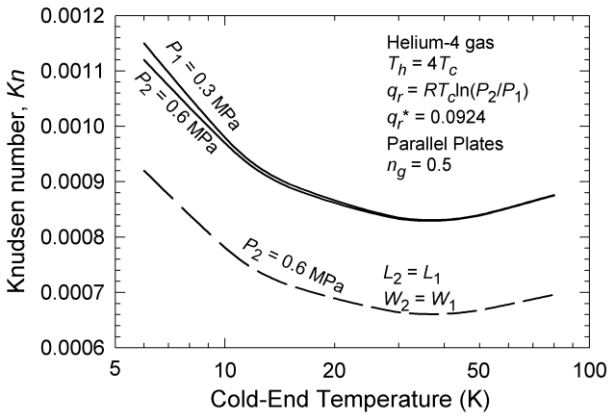

Figure 16. Knudsen number for both sides of the heat exchanger for case A.

these examples. For case B pure nitrogen is the working fluid operating between 80 K and 300 K with a low pressure of 0.1 MPa and a high pressure of 15 MPa provided by the compressor at the warm end of the heat exchanger. The pressure ratio of 150 is very high and requires a special compressor with several stages of compression. For case C the temperatures of 80 K and 300 K and the low pressure of 0.1 MPa are kept the same, but the high pressure is reduced to 2.5 MPa, which can be provided by conventional compressors used in household refrigerators. For case D a gas mixture of nitrogen and hydrocarbons operates between the 80 K and 300 K with 0.1 MPa and 2.5 MPa pressures. For case E helium gas operates between 0.3 and 0.6 MPa with temperatures of 6 and 18 K, and for case F helium has the same pressures as in case E but the temperatures are between 140 K and 300 K. In the last case the Joule-Thomson expansion will not provide any cooling because the temperature is above the inversion temperature. In this case we specify some fixed heat exchanger ineffectiveness 1 - ε and calculate the required external specific refrigeration power required according to equations (15) and (16) to absorb the heat flow at the cold end of the heat exchanger.

Table 2 gives the optimized geometry and other important parameters for the examples discussed above. The case designations of, for example B1, B2, B2*, correspond to (1) the low-

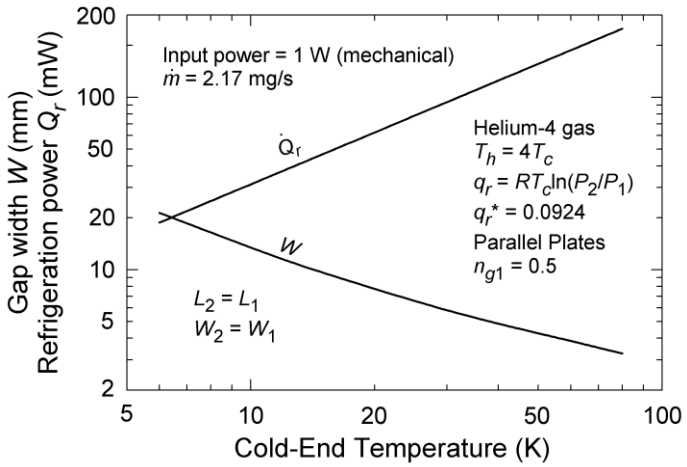

Figure 17. Gap width of parallel plates and the gross refrigeration power for case A with 1 W of mechanical input power as a function of cold end temperature.

Table 1. Input parameters used in example calculations of optimized recuperative heat exchangers.

Case	Gas	Cycle	T_c, T_h (K)	P_1, P_2 (MPa)	q_r (J/g)	q_r*	n_g	$\Delta P/P_0$	Q_{hx}/Q_r	Q_{cond}/Q_r
A	He	Isoth. exp.	$T_h = 4T_c$	0.3, 0.6	$1.440T_c$	0.0924	0.5	0.1	0.1	0.1
B	N_2	JT	80, 300	0.1, 15	26.57	0.1157	0.4	0.4, 0.1	0.1	0.1
C	N_2	JT	80, 300	0.1, 2.5	5.170	0.0224	0.4	0.4, 0.1	0.1	0.1
D	mix	JT	80, 300	0.1, 2.5	62.48	0.090	0.4	0.2, 0.1	0.1	0.1
E	He	JT	6, 18	0.3, 0.6	1.874	0.0253	0.4	0.1, 0.1	0.15	0.05
F	He	precool	140, 300	0.3, 0.6	8.309	0.01	0.4	0.05, 0.05	0.5	0.25

Table 2. Calculated optimum geometry and flow parameters for example heat exchangers.

Case	n_g	Q_{cond}/Q_r	A_g/m (cm^2s/g)	L (mm)	t_g (μm)	Kn	N_r	Q_r (mW)	m (mg/s)	W (mm)
B1	0.4	0.1	0.356	53.9	56.2	0.00066	255	10	0.376	0.238
B2	0.4	0.1	0.00496	0.75	0.925	0.00050	161	10	0.376	0.202
B2*	0.05	0.05	0.00496	47.5	7.36	0.00006	1284	10	0.376	0.025
C1	0.4	0.1	0.809	630	127.5	0.00029	254	10	1.934	1.23
C2	0.4	0.1	0.0648	50.4	16.6	0.00009	391	10	1.934	0.755
C2*	0.1	0.05	0.0648	605	35.2	0.00004	830	10	1.934	0.356
D1	0.4	0.1	0.0867	5.58	6.56	0.0395	39.9	10	0.160	0.212
D2	0.4	0.1	0.0164	1.06	3.27	0.00413	32.9	10	0.160	0.080
D2*	0.2	0.05	0.0164	5.64	7.55	0.00179	76.0	10	0.160	0.035
E1	0.4	0.05	0.309	6.88	3.56	0.00050	85.5	10	5.34	46.4
E2	0.4	0.05	0.139	3.09	2.21	0.00043	110	10	5.34	33.6
E2*	0.25	0.05	0.139	6.19	3.13	0.00031	155	10	5.34	23.7
F1	0.4	0.25	1.417	215	173	0.00026	151	-66.5	5.34	4.37
F2	0.4	0.25	0.709	108	86.7	0.00026	151	-66.5	5.34	4.36
F2*	0.25	0.25	0.709	215	123	0.00019	214	-66.5	5.34	3.09

pressure stream, (2) the high-pressure stream, and (3) the high-pressure stream with the length made the same as that of the low-pressure side. Matching the lengths is a practical requirement for most heat exchangers, but it does lead to an increase in the required volume. Matching the widths, as was done for case A, may also be a practical requirement in most cases, but that has not been done for the rest of the examples. There are several important points we wish to point out regarding the various examples. First, the gap thickness for all cases except C1, F1, and F2* are less than 100 μm. Thus, microscale heat transfer is of interest here. The optimum gap thickness decreases at lower temperatures. However, the Knudsen numbers for all cases except the mixed refrigerant case are less than 10^{-3}. Thus, slip flow is of little concern and the use of the friction factor and Stanton number correlations for continuum flow should be valid. The Reynolds numbers are much less than 2000, so the laminar flow assumption in calculating the hydraulic diameter is valid.

The need for high effectiveness heat exchangers in cryocoolers is indicated by the low values of q_r^*, which gives the maximum ineffectiveness allowed for the heat exchanger, at which point net refrigeration is eliminated. With pure gases in a Joule-Thomson (JT) cryocooler starting from

temperatures much above the normal boiling point, for example nitrogen at 300 K, very low ineffectiveness (<0.0224) is required to reach 80 K when the high pressure is only 2.5 MPa. That requirement leads to relatively large heat exchangers and difficulty in practice of actually achieving the very low ineffectiveness. The use of mixed refrigerants, as in case D, increases q_r^* to 0.090 for the same pressures and permits a reduction in the size of the heat exchanger. As shown by the results in Table 2 the Knudsen numbers for the mixed refrigerant case are rather large and indicate significant slip flow. However, the calculations for the mean free path were made assuming a gas phase, whereas both gas and liquid phases exist in much of the heat exchanger, especially in the high-pressure side. Thus, two-phase heat transfer becomes important here, and heat transfer will be enhanced beyond that assumed here for a single phase.

A JT cryocooler stage using helium with a pressure ratio of 2 can provide refrigeration at 6 K when the helium is precooled to about 18 K. Such JT stages are under development by two aerospace companies for 6 K cryocoolers for space applications [8]. Still, the ineffectiveness of the heat exchanger must be quite small (<0.0253). Stirling or pulse tube cryocoolers are used to precool the helium gas to 18 K. Case F represents an example of a heat exchanger for precooling helium gas from 300 K to 140 K as part of a system that uses case E for achieving 6 K. For this example the specific enthalpy difference between 300 K and 140 K for helium at either 0.3 MPa or 0.6 MPa is 8309 J/g. The flow rate is set from case E, which then gives the total heat transferred in the heat exchanger. For this case we must select some desired ineffectiveness on each side to determine the heat $\dot{Q}_{hx}$ from each side that must be absorbed at the cold end using equation (12). The resulting N_{tu} from published graphs can then be used directly in equation (11). For this case we arbitrarily select a total ineffectiveness of 0.015. To maintain consistency with the other examples we then choose $q_r^* = 0.010$ as the maximum ineffectiveness and $(\dot{Q}_{hx} / \dot{Q}_r) = 0.5$ on each side to give a total actual ineffectiveness of 0.010. According to equation (16) the specific refrigeration power must be q_r = 8.309 J/g. With $(\dot{Q}_{cond} / \dot{Q}_r) = 0.25$ on each side the total loss from both sides of the heat exchanger becomes $1.5q_r$ = 12.46 J/g. For a gross refrigeration power of 10 mW at 6 K (case E) the flow rate is 5.34 mg/s, which then causes a heat flow of 66.5 mW at the 140 K heat exchanger that must be absorbed by some other cryocooler. The gap thickness and length of this higher temperature heat exchanger is significantly larger than its 6 K counterpart mainly because of the much lower density at these higher temperatures.

The small size of the heat exchangers described here are an advantage in many applications besides the development of micro cryocoolers. The small size reduces the radiation heat load to the cold end and the conducted heat load through mechanical supports, particularly for space applications where rigid launch support is needed. The lower mass is also important for space applications. The achievement of ineffectiveness values less than 1% is difficult in practice because of problems with nonuniform flow in parallel channels. Figure 18 shows an example of a parallel plate heat exchanger designed for conditions similar to those for case F above, except for somewhat higher flows [9]. Flow paths are formed by photoetching completely through a foil of the proper thickness rather than relying on depth etching. These foils are alternated with a barrier foil and diffusion bonded to form the complete heat exchanger. The uniform gap thickness leads to more uniform flow in each channel. The measured ineffectiveness of this heat exchanger was about 2.7%, which was higher than the design value of about 0.5%. The difference was attributed to flow imbalances. Improvements in fabrication techniques can lead to even lower ineffectiveness in similar compact heat exchangers [9].

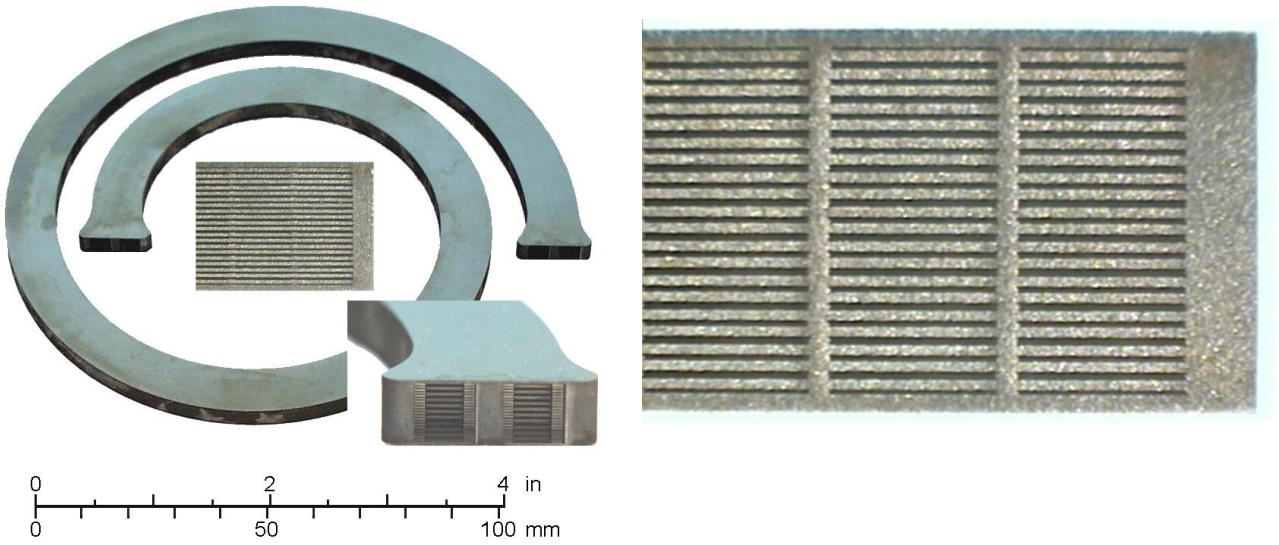

Figure 18. Photographs of a miniature heat exchanger developed for the precooling stage of a helium Joule-Thomson cryocooler. The construction used photoetched stainless steel foil diffusion bonded together [9].

6. Optimization of Regenerator Geometry and Frequency Limitations

As discussed in Section 2 the thermal penetration depth δ_t gives the effective distance oscillating heat flow can penetrate into any medium. According to equation (1) δ_t decreases with increasing frequencies. Thus, smaller hydraulic diameters are required at higher frequencies for good heat transfer within the helium working fluid. Also, in order to effectively utilize the heat capacity of the entire matrix volume for half-cycle heat storage the characteristic dimension of the matrix must also be less than δ_t for that material. As shown by figure 2 the thermal penetration depth in helium decreases at lower temperatures. For temperatures below about 20 K hydraulic diameters should be significantly less than about 50 μm for frequencies of about 10 Hz. The concept of a thermal penetration depth applies to conduction heat transfer, which is valid only in the laminar flow regime. However, we have seen in the previous section that for compact heat exchangers the Reynolds numbers are always much less than 2000. The same is true for regenerators.

6.1 ACOUSTIC OR PV POWER FLOW

The aspect of regenerative cryocoolers of interest here is their miniaturization, possibly for use in MEMS devices. The largest component of regenerative cryocoolers is the compressor, or pressure oscillator. The mechanical power, or PV power, output from the pressure oscillator is given by

$$\dot{W} = \tfrac{1}{2} P_1 \dot{V}_1 \cos\theta, \tag{49}$$

where P_1 is the amplitude of the sinusoidal pressure oscillation, $\dot{V}_1$ is the amplitude of the volume flow at the piston, and θ is the phase angle between the volume flow and the pressure. In terms of the total swept volume V_{co} (peak to peak) of the pressure oscillator the PV power is given by

$$\dot{W} = \tfrac{1}{2}\pi f P_1 V_{co} \cos\theta = \tfrac{1}{2}\pi f \left(\frac{P_r - 1}{P_r + 1} \right) P_0 V_{co} \cos\theta, \tag{50}$$

where f is the operating frequency and P_r is the pressure ratio (maximum divided by minimum). For a given power output the pressure oscillator size (proportional to swept volume) is reduced when increasing f or P_1 and keeping θ small. The pressure amplitude P_1 is increased when increasing the pressure ratio P_r or the average pressure P_0. Higher pressure ratios occur only by increasing the swept volume relative to the volume of the cold head, so that approach does not lead to reduced volumes. Pressure ratios in the range of 1.2 to 1.5 are typical for most high-frequency regenerative cryocoolers. We now examine the limits on the average pressure and the frequency.

As the average pressure increases the wall thickness and the solid fraction ($1 - n_g$) must increase. As indicated by equation (29) the solid fraction becomes significant for $P/\sigma \approx 0.1$. For higher pressures the outside dimensions will no longer decrease much. Typically the allowable tensile stress may be about 70 MPa, which gives an upper limit of about 7 MPa for the average pressure for any significant reduction in system size. As shown by equation (50) higher power densities in the pressure oscillator can be achieved with higher frequencies. Typically 60 to 70 Hz is about the maximum frequency currently being used, but that is not a limit set by the pressure oscillator. An upper frequency limit for the oscillator could be at least 1 kHz or more. The internal power density of the pressure oscillator according to equation (50) for an average pressure of 7 MPa, a pressure ratio of 1.3, a frequency of 1 kHz and a phase angle of 0 is 1.43 kW/cm^3. The ratio of external volume to the swept volume is of the order 10, so the maximum external power density is of the order 100 W/cm^3. There are questions regarding the upper limits to the power density of linear motors and whether they can provide this high a power density. However, as we shall see the regenerator has the major impact on the power density in the system, so we shall not dwell on the issues in the pressure oscillator.

The purpose of the regenerator is to transmit oscillating PV power, or acoustic power, from ambient temperature to some lower temperature with a minimum of losses. Just as with the recuperative heat exchangers discussed in section 5, the losses are those due to imperfect heat transfer $\dot{Q}_{reg}$, pressure drop ΔP, and conduction $\dot{Q}_{cond}$. The gross refrigeration power $\dot{Q}_r$ available at the cold end is simply the PV power delivered to the cold end whether the system is a Stirling or pulse tube cryocooler. There also would be some additional losses associated with the expansion process in the Stirling displacer or the pulse tube that are not part of the regenerator losses. Those losses may only be about 15 to 20% of the gross refrigeration power. Most of the losses are in the regenerator. Optimization of the regenerator geometry can be carried out much like that discussed in section 5 for recuperative heat exchangers. Regenerators have oscillating mass flows with an amplitude of $\dot{m}_1$. In most cases there is no steady or DC component of mass flow even though there is a steady-flow component of PV power from the compressor to the cold end of the regenerator. The relation between the time-averaged PV power flow and the mass flow amplitude for an ideal gas is given by

$$\dot{W} = \tfrac{1}{2} RT \left(P_1 / P_0 \right) \dot{m}_1 \cos\theta, \tag{51}$$

where θ is the phase angle between the flow and pressure and the relative pressure amplitude is related to the pressure ratio by

$$\frac{P_1}{P_0} = \frac{P_r - 1}{P_r + 1}. \tag{52}$$

6.2 GEOMETRY OPTIMIZATION

The optimization procedure to be discussed here uses some approximations that are good for temperatures above about 70 K, but are not very good for lower temperatures. For lower temperatures numerical analyses are necessary for good results. The amplitude of the pressure drop ΔP_1 for flow through the regenerator is given by equation (10) when $\dot{m}_1$ is used for the flow. The specific cross sectional area of the regenerator then becomes

$$\frac{A_g}{\dot{m}_1} = \left[\frac{N_{tu} N_{Pr}^{2/3}}{2\alpha \rho_0 \Delta P_1} \right]^{1/2}, \tag{53}$$

where ρ_0 is evaluated at the average pressure and temperature. There exists a relationship between the number of heat transfer units N_{tu} during peak flow and the regenerator thermal loss, but it is more complicated than that for recuperative heat exchangers. Numerical techniques must be used for the most general case. Kays and London [6] give a simplified expression that is a good approximation for temperatures of about 80 K and above. They show that the ineffectiveness of a regenerator is a function not only of N_{tu} but also of the heat capacity ratio between the matrix and the gas that passes through the regenerator. However, for temperatures of 80 K and above the volumetric heat capacity of nearly all matrix materials is much larger than that of helium gas. In that case the relation between the ineffectiveness and N_{tu} is the same as for recuperative heat exchangers given by equation (19). Because both the hot and cold blows flow through the same flow channel in a regenerator we have

$$N_{tu1} = N_{tu2} = N_{tu} = 2N_{tu0}. \tag{54}$$

Then according to equation (18) the total ineffectiveness of the regenerator is approximated by

$$1 - \varepsilon = 2B / N_{tu}. \tag{55}$$

Here B can be made greater than 1 to better approximate the case where the heat capacity ratio is not larger than about 10. For a heat capacity ratio of 2, equation (55) is still a good approximation with $B = 2$. The relationship between the ineffectiveness and the regenerator thermal loss is given by

$$1 - \varepsilon = (\dot{Q}_{reg} / \dot{Q}_r) q_r^*, \tag{56}$$

which is the same as for the recuperative heat exchanger given by equation (15).

The specific gross refrigeration power of the regenerative cryocooler is given by

$$q_r = \dot{Q}_r / \dot{m}_1 = \dot{W}_c / \dot{m}_1 = \tfrac{1}{2} R T_c \left(P_1 / P_0 \right) \cos\theta. \tag{57}$$

The relative refrigeration power for an ideal gas is then

$$q_r^* = \frac{2q_r}{h_h - h_c} = \frac{T_c (P_1/P_0)\cos\theta}{(c_p/R)(T_h - T_c)} \tag{58}$$

where the factor of 2 is used to account for the fact that the denominator refers to heat flow between the gas and the matrix for a half cycle whereas the numerator refers to the full cycle. With the same conditions as case A for recuperative heat exchangers we have $q_r^* = 0.0444\,(\theta = 0)$ compared with 0.0924 for the ideal recuperative cycle. With the more common pressure ratio of 1.3 instead of 2.0 we have $q_r^* = 0.0174$. Thus, the ineffectiveness of regenerators must be less than that of recuperative heat exchangers for the same fractional heat loss. That is relatively easy to accomplish in practice because of the simple construction of regenerators with only one flow stream. The specific gas cross-sectional area of the regenerator is then expressed as

$$\frac{A_g}{\dot{m}_1} = \left[\frac{BN_{Pr}^{2/3}}{\alpha\rho_0 q_r^* \Delta P_1 (\dot{Q}_{reg}/\dot{Q}_r)}\right]^{1/2}. \tag{59}$$

This equation is the same as equation (21) except for the factor of 2 in the denominator in equation (21). In this case $\dot{Q}_{reg}$ is for the complete regenerator whereas $\dot{Q}_{hx}$ in equation (21) is for one side of the heat exchanger. We note that the specific area is independent of frequency. Another assumption that is a part of equation (59) is that the amplitude of the mass flow rate is the same throughout the regenerator. In practice the flow rate may vary by 20 to 30% from one end to the other in an optimized design. The pressure drop in equation (59) can be made into a relative form ($\Delta P_1/P_1$) that equals the fractional loss of PV power and the gross refrigeration power. With that modification and with the ideal gas assumption equation (59) becomes

$$\frac{A_g}{\dot{m}_1} = \left[\frac{RT_0 BN_{Pr}^{2/3}}{\alpha q_r^* P_0^2 (P_1/P_0)(\Delta P_1/P_1)(\dot{Q}_{reg}/\dot{Q}_r)}\right]^{1/2}. \tag{60}$$

The calculations for the length and the hydraulic diameter of the regenerator are the same as for the recuperative heat exchangers. Thus, equation (28) gives the optimum length and equation (39) gives the optimum hydraulic diameter. They are repeated here for convenience:

$$L = \frac{(A_g/\dot{m}_1)(1-n_g)\int k_{eff}\,dT}{n_g q_r (\dot{Q}_{cond}/\dot{Q}_r)} \tag{28*}$$

$$D_h = \left[\frac{2b\mu(1-n_g)\int k_{eff}\,dT}{n_g\rho_0 q_r \Delta P_1 (\dot{Q}_{cond}/\dot{Q}_r)}\right]^{1/2}, \tag{39*}$$

where k_{eff} is the effective thermal conductivity of the matrix when the effect of multiple interfaces are taken into account, such as with stacked screen or packed spheres [10]. The gas volume in the regenerator is found by combining equations (59) and (28*) to give

$$\frac{V_{rg}}{\dot{m}_1} = \frac{A_g L}{\dot{m}_1} = \frac{BN_{Pr}^{2/3}(1-n_g)\int k_{eff}\,dT}{\alpha n_g q_r^* q_r \rho_0 \Delta P_1 (\dot{Q}_{reg}/\dot{Q}_r)(\dot{Q}_{cond}/\dot{Q}_r)}. \tag{61}$$

In general both $(\dot{Q}_{cond} / \dot{Q}_r)$ and $(\dot{Q}_{reg} / \dot{Q}_r)$ will be double the corresponding values for recuperative heat exchangers because they refer to the complete regenerator. With the ideal gas assumption the gas volume becomes

$$\frac{V_{rg}}{\dot{m}_1} = \frac{RT_0 BN_{Pr}^{2/3}(1-n_g)\int k_{eff}\,dT}{\omega n_g q_r^* q_r P_0^2 (P_1/P_0)(\Delta P_1/P_1)(\dot{Q}_{reg}/\dot{Q}_r)(\dot{Q}_{cond}/\dot{Q}_r)}. \tag{62}$$

This equation shows that for fixed relative losses, frequency has no effect on the volume, length or hydraulic diameter, but an increase in the average pressure for the same pressure ratio has a significant effect in decreasing the volume and a smaller effect on the hydraulic diameter. We can relate the mass flow rate to the total mass m_f (peak to peak) of gas that flows through the regenerator and out the ends by

$$\dot{m}_1 = \pi f m_f . \tag{63}$$

We can replace the mass of gas by the swept volume at either end of the regenerator. For the compressor end and with an ideal gas we have

$$\dot{m}_1 = \pi f P_0 V_{co} / RT_{co}, \tag{64}$$

where the compressor temperature T_{co} is usually equal to T_h. Substituting this expression for the flow rate into equation (62) gives us the gas volume ratio between the regenerator and the compressor as

$$\frac{V_{rg}}{V_{co}} = \frac{\pi f (T_0/T_{co}) BN_{pr}^{2/3}(1-n_g)\int k_{eff}\,dT}{\omega n_g q_r^* q_r P_0 (P_1/P_0)(\Delta P_1/P_1)(\dot{Q}_{reg}/\dot{Q}_r)(\dot{Q}_{cond}/\dot{Q}_r)}. \tag{65}$$

6.3 LIMITED MATRIX HEAT CAPACITY

In regenerators the porosity n_g of the matrix is not constrained by pressure considerations, but the overall porosity that includes the confining tube must not exceed the value given by equation (29). However, high values of the matrix porosity may lead to insufficient matrix heat capacity. The heat capacity ratio is given by

$$\frac{C_r}{C_f} = \frac{V_{rg}(1-n_g)\rho_m c_m}{n_g m_f c_p}, \tag{66}$$

where $\rho_m c_m$ is the volumetric heat capacity of the matrix, m_f is the total mass (peak to peak) of gas that flows through the regenerator, and c_p is the specific heat at constant pressure for the gas (usually helium). The total mass of fluid can be given by

$$m_f = \rho_{co} V_{co}, \tag{67}$$

where ρ_{co} is the density of the gas at the compressor temperature. Equation (66) can then be written as

$$\frac{C_r}{C_f} = \frac{(V_{rg}/V_{co})(1-n_g)(\rho_m c_m/\rho_0 c_p)(T_{co}/T_{ave})}{n_g}, \tag{68}$$

where T_{ave} is the average temperature of the regenerator. By using equation (63) for the fluid mass we can also express the heat capacity ratio as

$$\frac{C_r}{C_f} = \frac{\pi f (V_{rg} / \dot{m})(1 - n_g)\rho_m c_m}{n_g c_p}. \tag{69}$$

In order to use the relationship between ineffectiveness and N_{tu} given by equation (55) with $B = 1$, the heat capacity ratio must be at least 10. Even larger ratios are needed when the matrix specific heat drops rapidly with decreasing temperatures to account for a low ratio at the cold end of the regenerator. We now see that increasing frequency has the beneficial effect of increasing the heat capacity ratio, even though it has no effect on decreasing the gas volume in the regenerator according to equation (62). However, as we mentioned earlier, an increase in frequency does decrease the swept volume of the pressure oscillator, and in a like manner the swept volume at the cold end of the regenerator. The reduced swept volume at the cold end decreases the size the displacer in a Stirling cryocooler or the pulse tube in the pulse tube cryocooler.

6.4 FREQUENCY EFFECTS

So far in our analyses everything looks good as far as the use of increased pressures and frequencies to decrease the size of regenerative cryocoolers. An increased frequency and average pressure decreases the swept volume of the pressure oscillator and an increased average pressure decreases the size of the regenerator. We now calculate what happens when the frequency becomes too high. The frequency affects both the magnitude and the phase of the mass flow rate between the two ends of the regenerator. According to the mass conservation equation the mass flow at the hot end of the regenerator is related to the mass flow at the cold end by

$$\boldsymbol{\dot{m}_h} = \boldsymbol{\dot{m}_c} + \frac{d\boldsymbol{m_g}}{dt}, \tag{70}$$

where the bold variables are complex or phasor variables. For an ideal gas we have

$$\boldsymbol{\dot{m}_h} = \boldsymbol{\dot{m}_c} + \frac{\boldsymbol{\dot{P}} V_{rg}}{R T_r}, \tag{71}$$

where T_r is the log-mean temperature of the regenerator. For sinusoidal pressure oscillations of amplitude P_1 equation (71) becomes

$$\boldsymbol{\dot{m}_h} = \boldsymbol{\dot{m}_c} + \frac{i 2\pi f \boldsymbol{P_1} V_{rg}}{R T_r}, \tag{72}$$

where i is the imaginary unit. The second term on the right hand side of equation (72) is referred to as the compliance component and is analogous to capacitance in electrical systems. In an optimized design of regenerators the flow at the cold end lags the pressure in time and the flow at the warm end leads the pressure in time. The time derivative of the pressure $\boldsymbol{\dot{P}}$ forms the third leg of a roughly equal lateral triangle with the three phasors as shown in Figure 19. The magnitude of the compliance component is roughly the same as the other two terms in equation (72). In that case the magnitude of the mass flow rate does not vary much throughout the regenerator. However, as the frequency

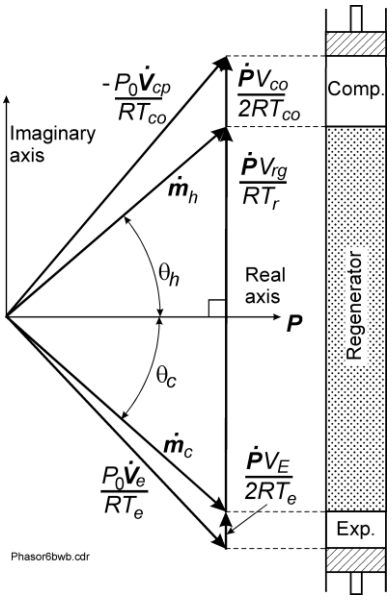

Figure 19. Phasor diagram for mass conservation in a Stirling cryocooler.

increases the vertical phasor in Figure 19 or the compliance component increases in proportion to the frequency. For $\dot{\boldsymbol{m}}_{\boldsymbol{c}}$ fixed (both amplitude and phase θ with respect to pressure) $\dot{\boldsymbol{m}}_{\boldsymbol{h}}$ increases (both amplitude and phase θ) as the frequency becomes large. The higher amplitude of the flow in the regenerator near the warm end then requires a larger regenerator area (taper) according to equation (60) and leads to an increase in the volume. We have performed extensive numerical analyses of regenerators and have shown that the system efficiency begins to decrease for phase angles at the warm end greater than about 50°. The higher flow rate and phase angle means that the swept volume of the compressor is increased for the same PV power according to equation (51). Thus, there is some upper limit to the frequency, beyond which volumes no longer decrease. To quantify this effect we divide equation (72) by the flow rate amplitude $\dot{m}_1$, which we consider to be the average amplitude throughout the regenerator. To keep the phase angle between the flow at either end and the pressure from becoming much larger than about 50° at the warm end we then require the compliance component to approximately satisfy the condition

$$\frac{2\pi f P_0 (P_1 / P_0)(V_{rg} / \dot{m}_1)}{RT_r} < \sqrt{2}. \tag{73}$$

This equation can be used to find the maximum $V_{rg} / \dot{m}_1$ for a given frequency or the maximum frequency for the calculated $V_{rg} / \dot{m}_1$. We recall that the calculated $V_{rg} / \dot{m}_1$ is independent of frequency. Substituting equation (62) into equation (73) gives the approximate upper limit to the frequency as

$$f < \frac{\alpha n_g q_r^* q_r P_0 (\Delta P_1 / P_1)(\dot{Q}_{hx} / \dot{Q}_r)(\dot{Q}_{cond} / \dot{Q}_r)}{\sqrt{2}\pi B N_{Pr}^{2/3} (1 - n_g) \int k_{eff}\, dT}. \tag{74}$$

For a given frequency the maximum $V_{rg}/\dot{m}_1$ is best expressed using the volume ratio

$$\frac{V_{rg}}{V_{co}} < \frac{1}{\sqrt{2}(P_1/P_0)(T_{co}/T_r)}, \tag{75}$$

where equation (64) for $\dot{m}_1$ was substituted into equation (73). An increase in frequency increases the volume ratio, but the maximum frequency given in equation (74) causes the ratio to reach the maximum given in equation (75). We now substitute this upper limit on the volume ratio into equation (68) to obtain an upper limit on the porosity that is given by

$$n_g < (n_g)_{\max} = \frac{\Omega}{1+\Omega}, \qquad \Omega = \frac{(\rho_m c_m/\rho_0 c_p)}{\sqrt{2}(P_1/P_0)(C_r/C_f)}, \tag{76}$$

where we made the assumption that $T_r \approx T_{ave}$. Figure 20 shows how the maximum porosity from equation (76) decreases with decreasing temperatures for $C_r/C_f = 100$. For these calculations the matrix volumetric heat capacity $\rho_m c_m$ was taken as a smooth curve representing the best available regenerator materials. For a regenerator with this maximum porosity the maximum frequency decreases with decreasing temperatures, as shown in Figure 21 where the conditions were taken as those of case G discussed in the next section. The various geometrical parameters, such as area, length, and hydraulic diameter can be calculated using the maximum porosity from equation (76).

6.5 EXAMPLES

The equations given above for regenerator optimization are reasonably accurate for temperatures above about 50 K. At lower temperatures real gas effects and the effect of compression and expansion of the gas within the regenerator cause additional heat transfer that makes these simple equations no longer valid. At lower temperatures numerical analyses are required to obtain reasonably accurate results[11]. These simple equations are useful for understanding the physics of the regenerative processes and for understanding the effect of various variables. The equations given here are used to examine several cases of regenerative cryocoolers. In all cases the regenerators are made with stainless steel. Some

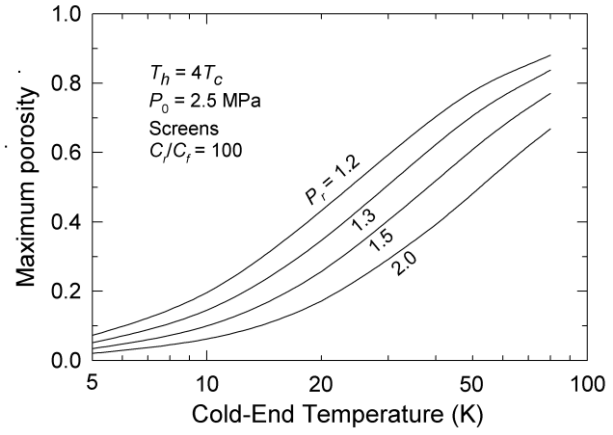

Figure 20. Calculated maximum porosity in screen regenerators as a function of cold end temperature in order to maintain adequate matrix heat capacity.

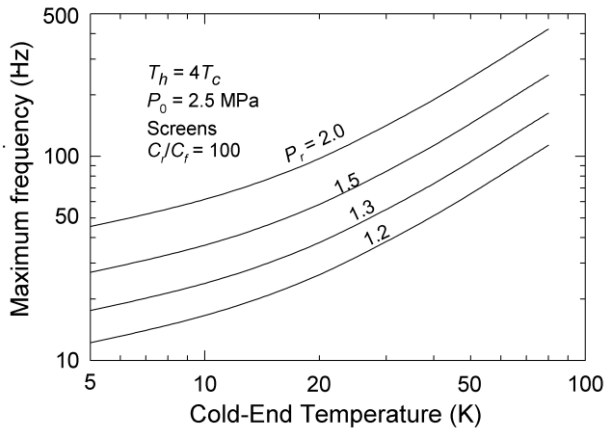

Figure 21. Calculated maximum frequency to prevent an excessive compliance in screen regenerators with the maximum porosity given in Figure 20.

cases use screen, which has a thermal conductivity degradation factor of 0.13 [10]. However we used a factor of 0.31 here to account for a combination of the screen and the tube containing the screen. Some cases use parallel plates, but we continue to use the conduction factor of 0.31 to make a clearer comparison between the two geometries.

Case G is typical of many Stirling or pulse tube refrigerators operating between 80 and 320 K. The input parameters are given in Table 3 and the results are given in Table 4. Case H is for the same conditions except the lower temperature is 40 K and the upper temperature is 160 K, which gives a temperature ratio of 4 as for case G. Some enhancement to the stainless steel heat capacity was made for this calculation to simulate the use of some improved regenerator material at this low temperature. Note that as the temperature is lowered the optimum hydraulic diameter decreases. Case I is for temperatures between 80 and 320 K, but with a lower pressure ratio. The lower pressure ratio increases the hydraulic diameter as expected from equation (39*) for the same relative pressure loss. The lower pressure ratio also decreases q_r. The relative losses given in Table 3 for case I match those found to maximize the overall efficiency of the cycle using numerical analyses [11], shown as case I* in the tables with data taken from REGEN3.2 run #2880. The geometrical parameters used in the numerical calculation are then compared with those calculated from the simple equations given here. The calculated values for the area and the length agree within about 10% with those of the numerical model, but the hydraulic diameter differs by about 25%. The 55.4 μm hydraulic diameter is achieved in practice with screen of #400 mesh with 25.4 μm wire diameter. Finer mesh screen suggested by the

Table 3. Input parameters used in example calculations for optimized regenerators.

Case	T_c, T_h (K)	P_0 (MPa)	P_r	f *(Hz)*	q_r (J/g)	q_r*	Geom.	n_g	$\Delta P_1/P_1$	Q_{reg}/Q_r	Q_{cond}/Q_r
G	80, 320	2.5	1.30	60	10.84	0.0166	screen	0.69	0.21	0.33	0.07
H	40, 160	2.5	1.30	60	5.42	0.0174	screen	0.69	0.21	0.33	0.07
I	80, 320	2.5	1.25	60	8.83	0.0142	screen	0.69	0.21	0.33	0.10
I*	80, 320	2.5	1.25	60	8.83	0.0142	screen	0.69	0.21	0.33	0.10
J	80, 320	8.0	1.50	400	16.6	0.0266	screen	0.69	0.21	0.33	0.07
K	80, 320	8.0	1.50	400	16.6	0.0266	plates	0.69	0.21	0.33	0.07
L	80, 320	8.0	1.50	400	16.6	0.0266	plates	0.20	0.21	0.33	0.07
M	80, 320	8.0	1.50	4000	16.6	0.0266	plates	0.69	0.21	0.33	0.07

Table 4. Calculated optimized geometry and flow parameters for example regenerators.

Case	A_g/m (cm^2s/g)	L (mm)	D_h (μm)	D_h/δ_t	N_r	C_r/C_f	f_{max} (Hz)	V_{rg}/V_{co}	W_h/A_t (W/cm^2)	Q_r (mW)	m_1 (mg/s)	d (mm)
G	0.801	44.8	41.0	0.29	33	177	69	2.54	37	10	0.923	0.370
H	0.566	22.5	19.5	0.24	35	40	97	1.81	26	10	1.85	0.441
I	0.962	46.3	41.2	0.29	28	219	66	3.15	25	10	1.13	0.449
I*	0.916	42.0	55.4	0.39	45	137	60	1.58	26	10	1.13	0.438
J	0.163	5.95	8.36	0.27	33	32	522	1.47	280	10	0.602	0.135
K	0.0586	2.14	6.47	0.21	71	4.1	4030	0.19	778	10	0.602	0.081
L	0.0586	18.7	19.1	0.61	211	14.4	461	1.66	227	10	0.602	0.150
M	0.0586	2.14	6.47	0.65	71	41	4030	1.90	778	10	0.602	0.081

equations given here is usually not commercially available.

Case J is an extreme case that attempts to miniaturize the overall system. In that case the average pressure is 8 MPa, the pressure ratio is 1.5, and the frequency is 300 Hz. Everything appears valid in that example including the maximum frequency of 522 Hz. The heat capacity ratio of 31.9 is somewhat low and may lead to a higher relative regenerator loss than 0.33 assumed here. Numerical analyses would be required to verify the results. Achieving the results of case J in practice will be difficult because of the problems associated with obtaining a hydraulic diameter of 8.36 μm in screen that has good flow and heat transfer characteristics. Further miniaturization is achieved by using parallel plates instead of screen, as shown in case K. Here the heat capacity ratio of 4.13 is far too low for the N_{tu} calculations to be valid. The use of lower porosity, 0.20, in case L helps to increase the heat capacity ratio to 14.4, but the size of the regenerator has increased. Case M is with the original porosity of 0.686, but the frequency is increased to 4000 Hz. The results in Table 4 show a heat capacity ratio of 133, which may be sufficient for high effectiveness, but numerical analyses would be needed to verify whether the regenerator behavior is dominated by heat transfer due to compression and expansion of the gas stored in the regenerator rather than by heat transfer due to the flow of gas through the temperature gradient. Even though the 4000 Hz frequency is very high and the time for heat transfer is very short, the classical correlations may still be valid because the 282 μm distance traveled by a parcel of gas at the cold end in case M is still large compared with the hydraulic diameter of 6.47 μm.

The PV power flux at the hot end of the regenerator $\dot{W}_h / A_t$ in Table 4 becomes very high for cases K and M. This power flow is equal to the heat that must be rejected to ambient before entering the regenerator. This is accomplished in an aftercooler whose volume must be small compared with that of the regenerator. Usually the diameter equals that of the regenerator and its length is much shorter. For a regenerator length of 2.14 mm in cases K and M the aftercooler should be no longer than about 0.5 mm. The heat flow density in this aftercooler then becomes 15.6 kW/cm^3, which is too high to be able to reject the heat without a very large temperature difference between the aftercooler and the ambient temperature heat sink. For comparison case G has a heat flow density of only about 40 W/cm^3, which is typical of present-day regenerative cryocoolers. This problem of rejecting heat to the environment becomes a serious problem in miniaturizing regenerative cryocoolers.

7. Conclusions

We have derived a set of simple equations to find the geometry of both heat exchangers and regenerators that minimizes their volume for a given refrigeration power. The equations are useful for the design of micro cryocoolers. With these equations we have shown that the optimum hydraulic diameters decrease with decreasing temperatures. For temperatures of 80 K and below the calculated hydraulic diameters are almost always less than 100 μm, and in some cases can be less than 5 μm. However, the Knudsen numbers are almost always less than 10^{-3}, which indicates slip flow does not occur and that continuum flow correlations from macrosystems can be used for analyses of these systems. The one exception may be in the use of mixed refrigerants, but that case is also complicated by the presence of two-phase flow. The use of mixed refrigerants in a Joule-Thomson cryocooler offers the potential of the smallest system for cooling to 80 K with no moving parts at the cold end. The equations developed for optimization of the heat exchangers show that for refrigeration powers

less than about 10 mW at 80 K the required gap width is about comparable to the gap thickness. Thus, for lower refrigeration powers, the optimization procedure described here is no longer valid.

The use of photoetched stainless steel foil diffusion bonded together was described as one fabrication method currently under study for developing miniature heat exchangers. Very uniform gap spacing is required to maintain uniform flow distribution and high effectiveness in the heat exchanger. Measured effectiveness was lower than the calculated value, which indicates a possible problem with non-uniform flow.

In regenerative cryocoolers, such as Stirling and pulse tube cryocoolers, the use of high frequency (>10 Hz) leads to thermal penetration depths in the helium working fluid that become less than about 100 μm at 80 K and even smaller at lower temperatures. For good heat transfer the regenerative heat exchangers (regenerators) must have hydraulic diameters significantly less than the thermal penetration depth. Thus hydraulic diameters less than 50 μm are commonly used in high frequency regenerative cryocoolers. Equations similar to those for recuperative heat exchangers were developed here and are useful for minimizing the volume of regenerators and the entire cryocooler. Correlations for steady flow should be valid for most cases with regenerative crycoolers because the amplitude of gas motion is usually much greater than the hydraulic diameter. Significant miniaturization of 80 K cryocoolers according to these equations can be achieved by the use of average pressures up to about 8 MPa and frequencies of 1 kHz or more. The required hydraulic diameters become less than 10 μm and represent a challenging fabrication problem. However, an even more serious problem is the very high heat flow density in the aftercooler, which makes it difficult to reject heat to ambient without a large temperature difference. Further research in miniaturizing regenerative cryocoolers would be useful and would require the use of numerical methods in the regenerator, particularly for temperatures below about 50 K where matrix heat capacities become low and real gas effects become pronounced.

REFERENCES

1. Bayazitoglu, Y., and Kakac, S., (2005) Flow Regimes in Microchannel Single-Phase Gaseous Fluid Flow, *Microscale Heat Transfer-Fundamentals and Applications*, S. Kakac (ed.), Kluwer Academic Publishers, Dordrecht (This publication).
2. Iguchi, M., Ohmi, M., and Maegawa, K., (1982) Analysis of Free Oscillating Flow in a U-Shaped Tube, *Bull. JSME*, Vol. 25, p.1398.
3. Kurzweg, U. H., Lindgren, E. R., and Lothrop, B., (1989) Onset of Turbulence in Oscillating Flow at Low Womersley Number, *Phys. Fluids A*, Vol. 1, pp. 1972-1975 and references therein.
4. Radebaugh, R., (2003) Cryocoolers and High-T_c Devices, *Handbook of High-Temperature superconductor Electronics*, N. Khare (ed.), Marcel Dekker, New York, pp. 379-424.
5. Radebaugh, R., (2003) Pulse Tube Cryocoolers, *Low Temperature and Cryogenic Refrigeration*, S. Kakac, *et al.* (eds.) Kluwer Academic Publishers, Dordrecht, pp. 415-434.
6. Kays, W. M., and London, A. L., (1984) Compact Heat Exchangers, third edition, McGraw-Hill, New York.

7. Radebaugh, R., Louie, B., (1985) A Simple, First Step to the Optimization of Regenerator Geometry, *Proceedings of the Third Cryocooler Conference*, NBS Special Publication 698, pp. 177-198.

8. Ross, R. G., and Boyle, R. F., (2003) NASA Space Cryocooler Programs – An Overview, *Cryocoolers 12*, R. G. Ross (ed.), Kluwer Academic/Plenum Publishers, New York, pp. 1-8.

9. Marquardt, E. D., and Radebaugh, R., (2003) Compact HighEffectiveness Parallel Plate Heat Exchangers, *Cryocoolers 12*, R. G. Ross (ed.), Kluwer Academic/Plenum Publishers, New York, pp. 507-516.

10. Lewis , M. A., and Radebaugh, R., (2003) Measurement of Heat Conduction Through Bonded Regenerator Matrix Materials, *Cryocoolers 12*, R. G. Ross (ed.), Kluwer Academic/Plenum Publishers, New York, pp. 517-522.

11. Gary, J., and Radebaugh, R., (1991) An Improved Numerical Model for Calculation of Regenerator Performance (REGEN3.1), *Proceedings of the 4th Interagency Meeting on Cryocoolers*, David Taylor Research Center DTRC-91/003, pp. 165-176.